

1 **Revision #3**

2
3 **Ordering kinetics in synthetic $\text{Mg}(\text{Al,Fe}^{3+})_2\text{O}_4$ spinels: quantitative elucidation of the whole**
4 **Al-Mg-Fe partitioning, rate constants, activation energies**

5 Filippo Parisi^{1,*}, Davide Lenaz², Francesco Princivalle² and Luciana Sciascia³

6 ¹ Dipartimento di Fisica e Chimica, University of Palermo, Viale delle Scienze, Parco d'Orleans II,
7 Ed. 17, 90128 Palermo, Italy

8 ² Dipartimento di Matematica e Geoscienze, University of Trieste, Via Weiss 8, 34127 Trieste,
9 Italy

10 ³ Dipartimento di Scienze della Terra e del Mare, University of Palermo, Via Archirafi 36, 90123
11 Palermo, Italy

12
13 **Abstract**

14 In this study, we report results of the application of a novel procedure for modeling cation ordering
15 in two synthetic $\text{Mg}(\text{Al}_{2-y}\text{Fe}^{3+}_y)\text{O}_4$ spinels ($y \sim 0.39$ and 0.54 , samples F39 and F54, respectively).
16 The kinetic profiles suggest a two-stage mechanism, with rapid inter-site exchange of Fe^{3+} with Mg
17 followed by slow exchange of Al with Mg. The trial to apply classical approaches, based on explicit
18 solutions of the differential equations corresponding to single-cation (Sha-Chappel model) or two-
19 cation (Müller model) exchange reactions, proved not feasible in the whole time range, thus
20 implying a lack of information about exchange processes involving the Fe^{3+} cation. Therefore we
21 decided to adopt an alternative methodology where a multistep pathway is simulated by Gepasi
22 modeling. The suggested set of reactions and the simultaneous solving of the related rate laws
23 allowed us to calculate rate constants and corresponding activation energies not only for the Al/Mg
24 cationic interchange (257 and 264 kJ/mol for the F39 and F54 samples, respectively), but also, for
25 the first time in such kind of samples (three cations - two sites), for the Fe/Mg cationic interchange
26 (204 and 234 kJ/mol for low- and high- Fe^{3+} samples, respectively).

27 The evaluation of the significant effect of the iron content, which actually inhibits Mg-Al
28 exchange between the T and M sites, provided new insights useful for the construction of
29 geothermometers based upon iron-bearing spinels.

30 Keywords: intersite cation exchange, spinels, kinetics, rate constant, activation energy,
31 geothermometers.

32

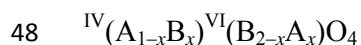
33

Introduction

34 The study of intersite cation exchange in rock-forming minerals constitutes a powerful tool for the
35 interpretation of thermodynamic properties and mixing behavior of solid solutions as well as for the
36 retrieval of the thermal history of host rocks (Ganguly 1982; Princivalle et al. 1999; Andreozzi et al.
37 2000; Ganguly and Stimpfl 2000; Müller et al. 2013). All these applications require a thorough
38 knowledge of both equilibrium distribution and exchange kinetics. Hence, in the last decades,
39 considerable effort has been devoted to the investigation of order-disorder processes in minerals
40 (e.g. Zema et al. 1999; Domeneghetti et al. 2000; Ganguly and Stimpfl 2000; Heinemann et al.
41 2000; Brizi et al. 2001; Wang et al. 2005) by means of complementary equilibrium and kinetics
42 studies.

43 In this context the study of cation distribution in spinels is fundamental for constraining the
44 geodynamic processes in which such minerals are involved (Della Giusta et al. 1986; Andreozzi et
45 al. 2000).

46 It is useful to recall that cation distribution in spinels can be described according to the general
47 scheme:



49 where A and B are bivalent and trivalent cations respectively, IV and VI refer to the coordination of
50 the T and M sites, respectively and x is the inversion parameter.

51

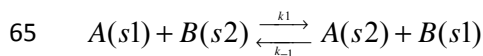
52 At low temperature, two ordered configurations of the spinel structure can be adopted: normal
53 configuration (e.g., MgAl_2O_4) with $x=0$, and inverse configuration (e.g., MgFe_2O_4), with $x=1$.

54 At high temperatures, a completely random distribution of A and B over the T and M sites is
55 expected for normal and inverse spinels ($x = 2/3$).

56 A detailed examination of the copious literature reveals that, as a consequence of the difficulties in
57 both gathering and interpreting the non-equilibrium data, the most critical point in obtaining a
58 comprehensive picture of the process, is the determination of the kinetic parameters. This issue has
59 been addressed by several authors with the aim of developing theoretical kinetic models with a wide
60 range of applicability.

61 Following the pioneering work of Bragg and Williams (1935) and Dienes (1955), Müller (1967,
62 1969) proposed a model for exchange kinetics based on a two-cation exchange reaction, which can
63 be generally expressed as:

64



66 where A and B are different cations, s_1 and s_2 are non-equivalent sites and k_1 and k_{-1} are kinetic rate
67 constants of the forward and backward reactions.

68 By solving the proper kinetic differential equations the following explicit solution for the site
69 occupancy as a function of time, $x(t)$, can be deduced (Brizi et al. 2001):

70

71

$$72 \quad x_i(t) = \frac{(b^2 - 4ac)^{1/2} \left(1 + \frac{(2ax_1 + b) - (b^2 - 4ac)^{1/2}}{(2ax_1 + b) + (b^2 - 4ac)^{1/2}} e^{-kt(b^2 - 4ac)^{1/2}} \right) - b \left(1 - \frac{(2ax_1 + b) - (b^2 - 4ac)^{1/2}}{(2ax_1 + b) + (b^2 - 4ac)^{1/2}} e^{-kt(b^2 - 4ac)^{1/2}} \right)}{2a \left(1 - \frac{(2ax_1 + b) - (b^2 - 4ac)^{1/2}}{(2ax_1 + b) + (b^2 - 4ac)^{1/2}} e^{-kt(b^2 - 4ac)^{1/2}} \right)}$$

73

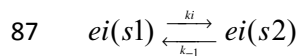
74 where x_1 is initial value of the site occupancy and a, b, and c depend on the composition of the
75 crystal and on the equilibrium distribution coefficient K_D .

76 Müller's model, as developed by Ganguly (1982), has been widely applied to model experimental
77 ordering-disordering data and estimate kinetic parameters (see for example Ganguly 1982; Sykes-
78 Nord and Molin 1993; Andreatzi and Princivalle 2002; Princivalle et al. 2012). However, despite
79 its success, it does not yield explicit general solution for ordering-disordering involving three or
80 more cations between two sites.

81 This limitation strongly hampers the application of the Müller's method to model experimental data
82 and estimate order-disorder kinetic coefficients, since several minerals have more than two cations
83 that can form solid solutions with ordering-disordering at each sites.

84 Among the numerous examples, spinels may be mentioned.

85 In the light of the limitations inherent in the Müller's model, Sha and Chappell (1996a, 1996b,
86 1997) proposed a kinetic model based on single-cation exchange reactions:



88 where ei is any cation involving in the ordering-disordering process.

89 In the case of a two-site system, the following kinetic equations can be deduced:

$$90 \quad x_1 = \frac{k_{21}m^0}{k_{12} + k_{21}} + \frac{k_{21}x_2^0 - k_{12}x_1^0}{k_{21} + k_{12}} e^{(-k_{12}-k_{21})t}$$

$$91 \quad x_2 = \frac{k_{12}m^0}{k_{21} + k_{12}} + \frac{k_{12}x_1^0 - k_{21}x_2^0}{k_{21} + k_{12}} e^{(-k_{12}-k_{21})t}$$

92 where x_1 and x_2 are the site occupancies of the cation in the two sites, k_{12} and k_{21} are the direct and
93 inverse kinetic constant and $m^0 = x_1 + x_2$.

94 It is important to point out that, although this second approach is suitable for both binary and multi-
95 cation ordering-disordering, it does not take into account that the rate of cation exchange reaction at

96 two non-equivalent sites depends on all the cations involved in the process. In other words, for a
97 three component system the rate constant value for the cation exchange of cation A at sites s1 and
98 s2 depends on whether the cationic exchange occurs with cation B or C, and it will be different in
99 the various cases.

100 In light of these considerations, in the present work we propose an alternative and highly versatile
101 methodology, based on numerical kinetics simulations. As case study to test the suitability of our
102 approach, we choose to apply it to model experimental ordering-disordering data in two synthetic
103 $\text{Mg}(\text{Al}_{2-y}\text{Fe}^{3+}_y)\text{O}_4$ spinels ($y \sim 0.39$ and 0.54 , samples F39 and F54, respectively), already presented
104 by Princivalle et al (2012).

105 For the purposes of the present work, the system $\text{Mg}(\text{Al},\text{Fe}^{3+})_2\text{O}_4$ is of particular interest, since,
106 although it has been observed that the Fe^{3+} content significantly influences the kinetics of ordering
107 process (Carbonin et al. 2002; Martignago et al. 2003, 2006; Princivalle et al. 2006), the
108 employment of classical methods allowed only the Al/Mg exchange reactions to be considered. As
109 a result, no information about the processes involving the Fe^{3+} cation could be obtained. The
110 procedure here proposed enabled us to evaluate the effect of the Fe^{3+} cation into Mg/Al cation
111 exchange processes, contributing to a closer reconstruction of host rocks thermal history.

112

113

Experimental

114 Set-up and experimental data here treated were presented in Princivalle et al. (2012). The samples
115 used in the present study are two synthetic spinels with the following composition:

116 $\text{Mg}_{1.0}\text{Fe}_{0.39}\text{Al}_{1.61}\text{O}_4$ (**sample F39**) and $\text{Mg}_{1.0}\text{Fe}_{0.54}\text{Al}_{1.46}\text{O}_4$ (**sample F54**).

117 They have been synthesized by flux-growth method and come from the same runs already analyzed
118 by Andreozzi et al. (2001) and Martignago et al. (2006). Synthesis procedure is shown in Andreozzi
119 (1999). Mössbauer and optical absorption spectroscopies performed by Andreozzi et al. (2001)

120 proved they are stoichiometric. The kinetics of cation ordering has been investigated by means of
121 quench method and X-ray single crystal diffraction. In particular, the distribution of Mg, Al and Fe
122 cations between T and M sites of the spinel structure has been investigated at three different
123 temperatures (550, 650, 750 °C) starting from an equilibrium ordering state corresponding to
124 1000°C, through several time-steps in order to monitor the rate of cation distribution. In detail,
125 crystals were disordered at 1000°C with an annealing time of 24 hours and then ordered at three
126 temperatures (550, 650, 750 °C), for different isothermal time-steps. After each annealing and
127 quenching experiment, crystals were mounted on a single crystal diffractometer for X-ray data
128 collection, and then subjected to the next experimental cycle by sealing the crystals in a thin-walled
129 quartz tube and putted directly at the wished temperature in the vertical tube furnace.

130 The modeling process were carried out by adopting a simulation method implemented in the Gepasi
131 software package (Mendes 1993; Mendes 1997; Mendes and Kell 1998). The first step of the
132 modeling procedure consists in building of the kinetic mechanism, which, in the present case,
133 implies the definition of the proposed interaction exchange reactions, their kinetic type (kinetic
134 differential equations describing the rate laws) and initial values of the site occupancies. In a second
135 step, experimental kinetic data (cationic occupancies as a function of time , $x_i(t)$) were fitted on the
136 basis of the proposed model by means of the optimization of the kinetic rate constant values.
137 Numerical Levenberg-Marquardt (LM) (Levenberg 1944; Marquardt 1963) method were applied to
138 simultaneously solve the systems of differential equations associated to each step. It is worth to say
139 that LM method is widely adopted in nonlinear regression problems where explicit form of $f(x)$
140 ($x_i(t)$ in the present study) is not available (Mendes and Kell 1998)

141

142

143

144

Results and discussion

145 Figures 1,2 and 3 report experimental site occupancies of the three cations (Mg, Al, Fe³⁺) at T and
146 M sites, expressed in atoms per formula unit (a.p.f.u.) as a function of time . At all the experimental
147 temperatures, two different reaction path can be recognized. In the first part of the kinetic profile,
148 we observe an Fe³⁺ increase at the T site balanced by Mg²⁺ increase at the M site, while in the
149 second part the opposite trend can be recognized. As for the Al³⁺ cation, a roughly monotonic
150 increase at the M site is observed. Since, obviously Mg, Fe and Al exchange start simultaneously,
151 the observation of the two distinct trend is due to different rate constants of the involved processes.

152 Supplementary evidence for the occurrence of the two reaction steps is the trend of the unit-cell
153 parameter (*a*) with time reported in Figure 4, where an initial decrease of *a* followed by a slower
154 increase is recorded.

155 This behavior can be interpreted by considering that in the first part of the kinetic profile, the two
156 samples are far from equilibrium and mostly behave as inverse spinel magnesioferrite
157 $T(Fe^{3+})^M(Mg,Fe^{3+})O_4$. In fact, according to previous studies (Mozzi and Paladino 1963; O'Neill et
158 al. 1992; O'Neill and Dollase 1994; Harrison and Putnis 1999; Andreozzi et al. 2001) the cation
159 distribution of MgFe₂O₄ spinel is random at high temperature and becomes gradually more ordered
160 (i.e, inversion increases) at low temperature. Therefore, for both F39 and F54 spinels starting from
161 random distribution, Mg²⁺ cations tend to occupy M site by exchanging with Fe³⁺ ions which tend to
162 fill T site. It is interesting to note that this behavior is particularly evident at the lowest temperature
163 (550 °C).

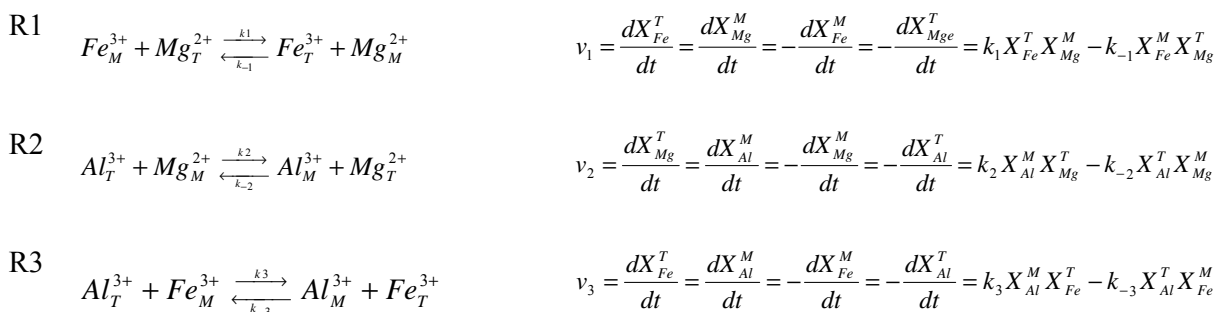
164 In the second part of the kinetic profile, approaching the equilibrium pertinent to the experimental
165 isotherm, the two samples behave as normal spinel sensu stricto $T(Mg)^M(Al_2)O_4$ and the exchange
166 of Mg vs. Al, become dominant.

167 As already mentioned in the introduction section, the classical approach to the analysis of such
 168 experimental data, based on the Müller's kinetic model, required that only the second part of the
 169 isotherm path, where the exchange of Mg vs. Al predominates, would be considered. This way, no
 170 information about the first rapid exchange could be obtained.

171 On the other hand, the trial to apply the model of Sha-Chappel also failed, since in the case of two-
 172 site systems, it is not able to reproduce experimental kinetic profiles characterized by the presence
 173 of maxima and minima (Sha and Chappell, 1997).

174 In light of the above considerations, in the present work, we performed the analysis of the
 175 experimental kinetic data by means of the Gepasi kinetic simulator, which allows the simultaneous
 176 solving of the relevant rate laws (v) corresponding to the proposed reactions steps.

177 In particular, we propose the following multistep reaction scheme (Scheme 1)



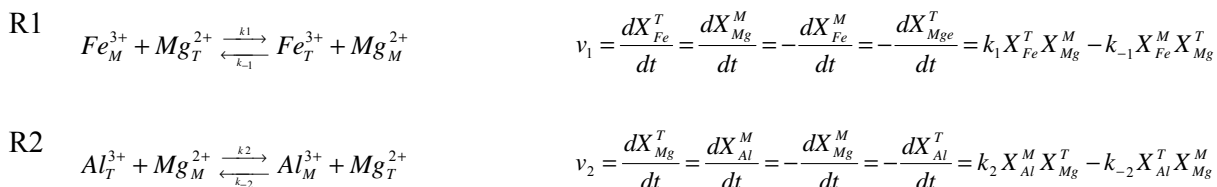
178

179 Scheme 1. Proposed reaction path and corresponding rate laws. k1, k2, k3 stand for ordering, and k-
 180 1, k-2 and k-3 stand for disordering processes.

181

182 In order to obtain the rate constant values, we applied the Levenberg-Merquardt method, as
 183 implemented in the Gepasi software, to solve the rate laws.

184 First of all, it has been observed that the best fit of the experimental data is obtained when the
185 kinetic rate constants associated with reaction R3 (forward and backward) reduce close to zero,
186 which can be reasonably interpreted by assuming that the direct exchange between Al and Fe does
187 not occur or is negligible in comparison with the other two cationic exchanges. Therefore the
188 following contracted reaction scheme (Scheme 2) has been tested, where the faster Fe/Mg intersite
189 exchange reaction (R1) is followed by the slower intersite Al/Mg exchange reaction (R2):



190 Scheme 2. Proposed reaction path and corresponding rate laws. k_1 , k_2 stand for ordering, and k_{-1} , k_{-2}
191 stand for disordering processes.

192 The proposed two-stage kinetic mechanism was hypothesized by Harrison et al. (1999), Martignago
193 et al. (2003, 2006) and Marinoni et al. (2011) for both natural and synthetic $Mg(Al,Fe)2O_4$ with
194 different iron content, and by Princivalle et al. (2012) for present samples.

195 This two-steps model completely reproduces the kinetic data (site occupancies versus time) in the
196 whole compositional and time range as can be easily observed in Figures 1-3 and in Figures S3 and
197 S4 in support of the manuscript, where the experimental kinetic profiles are reported together with
198 the simulated data in linear and logarithmic scale, respectively.

199 According to Merli et al. (2010) and to Merli and Sciascia (2011) the goodness of fit of the
200 simulation process is confirmed not only by the low values of the Residual Sum of Squares (mean
201 value ~ 0.0001) and Root Mean Squares Error (mean value ~ 0.001) but also by the negligible time
202 trend exhibited by residuals plots (Figures S5-S6 in support of the manuscript).

203 The simultaneous solution of the rate laws associated with the two steps of the Scheme 2 allowed us
204 to estimate the kinetic constants reported in Table 1, which support the hypothesis that the fastest

205 reaction step involves the Fe/Mg ionic couple (R1), while the step involving the Al/Mg ionic
206 exchange (R2) is slightly slower. On the other hand it can be observed that the differences between
207 k_1 and k_2 at the three investigated temperature is not so high, suggesting that the two processes
208 does not occurs on different time scale.

209 However, despite the probable correlation between the two processes, a quite good accordance
210 between the values here obtained for the kinetic rate constants relative to the Al/Mg exchange and
211 those previously reported by Princivalle et al.(2012), where this correlation is neglected, has to be
212 noticed.

213 As for the effect of the iron content in the two samples, it can be noted that the kinetic rate constants
214 are always higher for sample F54, indicating that the presence of the Fe^{3+} triggers the ionic
215 exchange between Mg and Al over T and M (Martignago et al. 2006).

216 In order to further corroborate the validity of the proposed model, the behavior of the a-parameter,
217 calculated according to the procedure described in Lavina et al. (2002), has been also successfully
218 simulated (see Fig.4).

219 In a second step of the present work, the temperature dependence of the kinetic constant k_i has been
220 employed to construct the Arrhenius plot reported in Figure 5.

221 The slope of the Arrhenius plot allowed us to calculate the activation energy values reported in
222 Table 2.

223 First of all, we can observe that, according to the trend of the kinetic rate constants and keeping
224 with the proposed model, the activation energy values corresponding to Fe-Mg ordering (E_{a1}) are
225 lower than those corresponding to Al-Mg ordering process (E_{a2}).

226 The higher activation energy corresponding to Al-Mg exchange agrees with the results of Marinoni
227 et al. (2011) who found that Al^{3+} is involved in the intra-crystalline cation partitioning only at high
228 temperatures, which means that the activation energy associated with the aluminium diffusion is
229 quite high. Intriguingly, this “retarding” effect is observed only when Fe^{3+} is present, which can be

230 taken as an indication of the reliability of the proposed kinetic mechanism which predicts that ferric
231 ions tend to keep the Mg ions in the M site, thus hampering cationic exchange with the Al cations.

232 With regards to Fe-Mg cation ordering, it can be observed that the obtained activation energy values
233 increase with increasing Fe³⁺ content in both samples. In the light of the decreased Al content, this
234 trend can be interpreted as follows:

- 235 1- the higher Fe³⁺ content implies a lower Al amount due to the substitution Fe³⁺ for Al;
- 236 2- as Al shows a site preference for M site, Mg accommodates at T site facilitating the
237 occurrence of the Mg/Fe cationic interchange (R1);
- 238 3- the higher is the Al content (F39 sample) the lower is the activation energy for the R1
239 process.

240 However, a comparison with the Ea values reported in literature for the synthetic MgFe₂O₄ end-
241 member (Harrison and Putnis 1999) indicates that the influence of Al on the Mg/Fe exchange is
242 quite limited. For example Ea1 is lowered of only 6% with respect to MgFe₂O₄ at more than 80% of
243 substitution (see Figure 6A, where the activation energy is reported as a function of the Al content,
244 for a clearer view of this data)

245 As for the Mg-Al exchange reaction, perusal of the data reported in Table 2 indicates that the
246 activation energy values (Ea2) obtained in present study for the F39 and F54 samples are higher
247 than those reported in literature for the MgAl₂O₄ end-member and, also in this case, they increase
248 on increasing the iron content. Again, this result is a further proof of the inhibition of the Al/Mg
249 cationic interchange due to the presence of the Fe³⁺ ions. It is interesting to note (see Figure 6B)
250 that the presence of ferric ions has a very strong influence in the Mg-Al exchange process(Ea2 is
251 increased of 34% with respect to MgAl₂O₄ at only 27% of substitution).

252 As already observed for the kinetic rate constant values, the accordance with the results of
253 Princiville et al. (2012) is reasonably high. However the trend of the Ea values as a function of iron
254 content obtained in the present work is more in line with the activation energy previously obtained

255 for the corresponding end-member. This can be taken as a proof of the higher capability of the
256 model here proposed to take into account the significant effect of the third cation.

257 This result could have important petrological implications in the construction of geothermometers
258 based upon the distribution of Mg and Al between the T and M sites of spinels containing Fe^{3+} (see
259 below).

260

261

Implications

262 Spinel is an important accessory mineral of several mafic and ultramafic rocks mainly constituted
263 by olivines \pm pyroxenes. These silicate minerals can be usually subjected to different degrees of
264 alteration and weathering so that spinel may be present as the sole-surviving primary mineral
265 (Lenaz et al. 2014).

266 As seen above, the Mg and Al ordering may give information on the thermal history of the host
267 rock. The importance of these minerals as petrogenetic indicators is therefore straightforward
268 (Irvine 1965 and Perinelli et al. 2014).

269 .

270 Because the question of whether the presence of additional major cations, usually present in natural
271 spinels (especially chromium and iron), affects, to a significant extent, the Mg-Al ordering,
272 Princivalle et al. (1999) introduced a geothermometer for intra-crystalline equilibration
273 temperatures based upon the distribution of Mg and Al between the T and M sites in Cr-spinel,
274 considering in the thermometer equation some coefficients taking into consideration the presence of
275 minor amount of other cations. A review of the recent literature seems to suggest that for low Fe-Cr
276 containing samples the investigation of the partitioning of Mg and Al cations still yield reliable
277 values for the closure temperatures. In fact this model has been successfully used in spinels in
278 which the total iron content is less than 0.25 a.p.f.u. and the chromium content is less than 1 a.p.f.u.

279 (Uchida et al. 2005; Lenaz et al. 2010, 2014; Princivalle et al. 2014 among the others). Anyway, in
280 natural spinels, very high Fe^{3+} contents yield unreliable temperatures in the range 1400-1900°C
281 (Lenaz et al. 2011; Derbyshire et al. 2013). In the light of the above considerations, the relevance
282 of the results obtained in the present study can be evaluated under different perspectives. First, the
283 acquired data reveal that the high amount of Fe^{3+} , tending to remain in the T site, affects the kinetic
284 parameters of Mg/Al exchange processes by hampering the Mg-Al exchange between the T and M
285 sites. This is a further evidence that geothermometers constructed by neglecting the processes
286 involving the iron ions (see for example the above discussed geothermometer by Princivalle et al.,
287 1999) should be carefully considered, especially when there is a high amount of Fe^{3+} in the studied
288 spinels. In this view, the present study represents a novelty, since the kinetic parameters here
289 provided are not affected by a priori assumptions and can be employed for the construction of
290 reliable geothermometers.

291

292

Acknowledgements

293 The authors wish to thank the University of Trieste and the MURST grants (FPr, PRIN 2010-2011 –
294 2010EARRRZ_006) for financial support. Great thanks are due to Professor em. Hans Annersten
295 and Professor Giovanni B. Andreozzi for their invaluable reviews, comments and suggestions,
296 which have improved the manuscript.

297

References

298

299 Andreozzi, G.B. (1999) Synthetic spinel in the $(\text{Mg}, \text{Fe}^{2+}, \text{Zn})(\text{Al}, \text{Fe}^{3+})_2\text{O}_4$ system: I. Flux growth
300 of single crystals. *Periodico di Mineralogia*, 68, 43-51.

301 Andreozzi, G.B. and Princivalle, F. (2002) Kinetics of cation ordering in synthetic MgAl_2O_4 spinel.
302 *American Mineralogist*, 87, 838–844.

- 303 Andreozzi, G.B., Princivalle, F., Skogby, H., and Della Giusta, A. (2000) Cation ordering and
304 structural variations with temperature in MgAl_2O_4 spinel: an X-ray single-crystal study.
305 American Mineralogist, 85, 1164-1171.
- 306 Andreozzi, G.B., Hålenius, U., and Skogby, H. (2001) Spectroscopic active $^{\text{IV}}\text{Fe}^{3+}$ - $^{\text{VI}}\text{Fe}^{3+}$ clusters
307 in spinel-magnesioferrite solid solution crystals: a potential monitor for ordering in oxide
308 spinels. Physics and Chemistry of Minerals, 28, 435-444.
- 309 Bragg, W.L. and Williams, E.J. (1935) The effect of thermal agitation on atomic arrangement in
310 alloys. Proceedings of Royal Society of London, 151A, 540-566.
- 311 Brizi, E., Molin, G., Zanazzi, P.F., and Merli, M. (2001) Ordering kinetics of Mg-Fe^{2+} Exchange in
312 a $\text{Wo}_{43}\text{En}_{46}\text{Fs}_{11}$ augite. American Mineralogist, 86, 271-278.
- 313 Carbonin, S., Martignago, F., Menegazzo, G., and Dal Negro, A. (2002) X-ray single-crystal study
314 of spinels: in situ heating. Physics and Chemistry of Minerals, 29, 503-514.
- 315 Della Giusta, A., Princivalle, F., and Carbonin, S. (1986): Crystal chemistry of a suite of natural Cr-
316 bearing spinels with $0.15 < \text{Cr} < 1.07$. Neues Jahrbuch für Mineralogie - Abhandlungen,
317 155, 319-330
- 318 Derbyshire E.J., O'Driscoll B., Lenaz D., Gertisser R., and Kronz A. (2013) Compositionally
319 heterogeneous podiform chromitite in the Shetland Ophiolite Complex (Scotland):
320 Implications for chromitite petrogenesis and late-stage alteration in the upper mantle portion
321 of a supra-subduction zone ophiolite. Lithos 162-163:279-300.
- 322 Dienes, G.L. (1955) Kinetics of order-disorder transformation. Acta Metallurgica, 3, 549-557.
- 323 Domeneghetti M. C., Molin G. M., Triscari M., and Zema M. (2000) Orthopyroxene as a
324 geospeedometer: Thermal history of Kapoeta, Old Homestead 001 and Hughes 002
325 howardites. Meteoritics and Planetary Science, 35, 347-354.

- 326 Ganguly J. (1982) Mg–Fe order-disorder in ferromagnesian silicates: II. Thermodynamics, kinetics
327 and geological applications. In: Advances in Physical Geochemistry, Ed. S. K. Saxena, Vol.
328 2 Springer-Verlag, New York, 58–99.
- 329 Ganguly, J. and Stimpfl, M. (2000) Cation ordering in orthopyroxenes from two stony-iron
330 meteorites: Implications for cooling rates and metal-silicate mixing. *Geochimica et*
331 *Cosmochimica Acta*, 64, 1291–1297.
- 332 Harrison, R.J., Dove, M.T., Knight, K.S. and Putnis, A. (1999) In-situ neutron diffraction study of
333 non-convergent cation ordering in the $(\text{Fe}_3\text{O}_4)_{1-x}(\text{MgAl}_2\text{O}_4)_x$ spinel solid solution. *American*
334 *Mineralogist*, 84, 555-563.
- 335 Harrison, R.J. and Putnis, A. (1999) Determination of the mechanism of cation ordering in
336 magnesioferrite(MgFe_2O_4) from the time- and temperature dependence of magnetic
337 susceptibility. *Physics and Chemistry of Minerals*, 26, 322-332.
- 338 Heinemann, R., Kroll, H., Langenhorst, F., and Lueder, T. (2000) Time and temperature variation
339 of the intracrystalline Fe^{2+} , Mg fractionation in Johnstown meteoritic orthopyroxene.
340 *European Journal of Mineralogy*, 12, 163-176.
- 341 Irvine, T.N. (1965) Chromian spinel as a petrogenetic indicator. *Canadian Journal of Earth*
342 *Sciences*, 2, 648-672.
- 343 Lavina, B., Salviulo, G., and Della Giusta, A. (2002) Cation distribution and structure modelling of
344 spinel solid solutions, *Physics and Chemistry of Minerals*, 29, 10-18.
- 345 Lenaz, D., De Min, A., Garuti, G., Zaccarini, F., and Princivalle F. (2010) Crystal chemistry of Cr-
346 spinels from the Iherzolite mantle peridotite of Ronda (Spain). *American Mineralogist*, 95,
347 1323-1328.
- 348 Lenaz, D., O’Driscoll, B., and Princivalle, F. (2011) Petrogenesis of the anorthosite – chromitite
349 association: crystal-chemical and petrological insights from the Rum Layered Intrusion, NW
350 Scotland. *Contributions to Mineralogy and Petrology*, 162, 1201-1213.

- 351 Lenaz, D., Youbi, N., De Min, A., Boumehdi, M.A., and Ben Abbou, M. (2014) Low intra-
352 crystalline closure temperatures of Cr-bearing spinels from the mantle xenoliths of the
353 Middle Atlas Neogene-Quaternary Volcanic Field (Morocco): A mineralogical evidence of a
354 cooler mantle beneath the West African Craton. *American Mineralogist*, 99, 267-275..
- 355 Levenberg, K. (1944) A method for the solution of certain nonlinear problems in least squares.
356 *Quarterly of Applied Mathematics*, 2, 164-168.
- 357 Marinoni, N., Levy, D., Dapiaggi, M., Pavese, A., and Smith, R.I. (2011) In situ high-temperature
358 X-ray and neutron powder diffraction study of cation partitioning in synthetic
359 $\text{Mg}(\text{Fe}_{0.5}\text{Al}_{0.5})\text{O}_4$. *Physics and Chemistry of Minerals*, 38, 11-19.
- 360 Marquardt, D.W. (1963). An algorithm for least squares estimation of nonlinear parameters. *SIAM*
361 *Journal on Applied Mathematics*, 11, 431-441.
- 362 Martignago, F., Dal Negro, A., and Carbonin, S. (2003) How Cr^{3+} and Fe^{3+} affect Mg-Al order
363 disorder transformation at high temperature in natural spinels. *Physics and Chemistry of*
364 *Minerals*, 30, 401-408.
- 365 Martignago, F., Andreozzi, G.B., and Dal Negro, A. (2006) Thermodynamics and kinetics of cation
366 ordering in natural and synthetic $\text{Mg}(\text{Al},\text{Fe}^{3+})_2\text{O}_4$ spinels from in situ high-temperature X-ray
367 diffraction. *American Mineralogist*, 91, 306-312.
- 368 Mendes, P. (1993) GEPASI: A software package for modelling the dynamics, steady states and
369 control of biochemical and other systems. *Computer Applications Biosciences*. 9, 563-571.
- 370 Mendes, P. (1997) Biochemistry by numbers: simulation of biochemical pathways with Gepasi 3.
371 *Trends in Biochemical Science*, 22, 361-363.
- 372 Mendes, P. and Kell, D.B. (1998) Non-linear optimization of biochemical pathways: applications to
373 metabolic engineering and parameter estimation. *Bioinformatics*, 14, 869-883.

- 374 Merli, M. and Sciascia, L. (2011) Iteratively reweighted least squares in crystal structure
375 refinements. *Acta Crystallographica Section A: Foundations of Crystallography*, 67, 456-
376 468.
- 377 Merli, M., Sciascia, L., and Turco Liveri, M.L. (2010) Regression diagnostics applied in kinetic
378 data processing: outlier recognition and robust weighting procedures. *International Journal*
379 *of Chemical Kinetics*, 142, 587-607.
- 380 Mozzi, R.L. and Paladino, A.E. (1963) Cation distributions in nonstoichiometric magnesium ferrite.
381 *Journal of Chemical Physics*, 39, 435–437.
- 382 Müller, R.F. (1967) Model for order-disorder kinetics in certain quasibinary crystals of
383 continuously variable composition. *Journal of Physics and Chemistry of Solids*, 28, 2239-
384 2243.
- 385 Müller, R.F. (1969) Kinetics and thermodynamics of intracrystalline distributions. *Mineralogical*
386 *Society of America Special Papers*, 2, 83-93.
- 387 Müller, T., Dohmen, R., Becker, H.W., ter Heege, J.H., and Chakraborty, S. (2013). Fe-Mg
388 interdiffusion rates in clinopyroxene: experimental data and implications for Fe-Mg
389 exchange geothermometers. *Contributions to Mineralogy and Petrology*, 166, 1563–1576.
- 390 O'Neill, H.St.C. and Dollase W.A. (1994) Crystal structures and cation distribution in simple
391 spinels from powder XRD structural refinements : MgCr_2O_4 , ZnCr_2O_4 , Fe_3O_4 and the
392 temperature dependence of the cation distribution in ZnAl_2O_4 . *Physics and Chemistry of*
393 *Minerals*, 20, 541-555.
- 394 O'Neill, H.St.C., Annersten, H., and Virgo, D. (1992) The temperature dependence of the cation
395 distribution in magnesioferrite (MgFe_2O_4) from powder XRD structural refinements and
396 Mössbauer spectroscopy. *American Mineralogist*, 77, 725–740.

- 397 Perinelli, C., Bosi, F., Andreozzi, G.B., Conte, A.M., Armienti, P. (2014) Geothermometric study of
398 Cr-spinels of peridotite mantle xenoliths from northern Victoria Land (Antarctica).
399 American Mineralogist, 99, 839-846.
- 400 Princivalle, F., Della Giusta, A., De Min, A., and Piccirillo, E.M. (1999) Crystal chemistry and
401 significance of cation ordering in Mg-Al rich spinels from high-grade hornfels (Predazzo-
402 Monzoni, NE Italy). Mineralogical Magazine, 63, 257-262.
- 403 Princivalle, F., Martignago, F., and Dal Negro, A. (2006) Kinetics of cation ordering in natural
404 $Mg(Al,Cr^{3+})_2O_4$ spinels. American Mineralogist, 91, 313-318.
- 405 Princivalle, F., Martignago, F., Nestola, F., and Dal Negro, A. (2012) Kinetics of cation ordering in
406 synthetic $Mg(Al, Fe^{3+})_2O_4$ spinels. European Journal of Minerals, 24, 633–643.
- 407 Princivalle, F., De Min, A., Lenaz, D., Scarbolo, M., and Zanetti, A. (2014) Ultramafic xenoliths
408 from Damaping (Hannuoba region, NE-China): petrogenetic implications from crystal
409 chemistry of pyroxenes, olivine and Cr-spinel and trace element content of clinopyroxene.
410 Lithos, 188, 3-14.
- 411 Redfern, S.A.T., Harrison, R.J., O'Neill, H.St.C., and Wood, D.R.R. (1999) Thermodynamics and
412 kinetics of cation ordering in $MgAl_2O_4$ spinel up to 1600 °C from in situ neutron diffraction.
413 American Mineralogist, 84, 299–310.
- 414 Sha, L.K. and Chappell, B.W. (1996a) Two-site multi-cation ordering-disordering in minerals: An
415 alternative kinetic model. American Mineralogist, 81, 881-890.
- 416 Sha, L.K. and Chappell, B.W. (1996b) A kinetic model for three-site intracrystalline ordering-
417 disordering in minerals. Geochimica et Cosmochimica Acta, 60, 2075-2086.
- 418 Sha, L.K. and Chappell, B.W. (1997) Multi-site order-disorder kinetics in crystalline solids: A
419 generalized formulation, American Mineralogist, 82, 325-336.
- 420 Sykes-Nord, J.A. and Molin, G.M. (1993) Mg-Fe order-disorder reaction in Fe-rich orthopyroxene :
421 structural variation and kinetics. American Mineralogist, 78, 921-931.

422 Uchida, H., Lavina, B., Downes, R.T., and Chesley, J. (2005) Single-crystal X-ray diffraction of
 423 spinels from the San Carlos Volcanic Field, Arizona: Spinel as a geothermometer. American
 424 Mineralogist, 90,1900-1908.

425 Wang, L, Moon, N., Zhang, Y., Dunham, W.R.,and Essene, E.J. (2005) Fe-Mg order-disorder in
 426 orthopyroxenes” Geochimica et Cosmochimica Acta, 69, 5777–5788.

427 Zema, M., Domeneghetti, M. C., and Tazzoli, V. (1999) Order-Disorder Kinetics In Orthopyroxene
 428 With Exsolution Products. American Mineralogist, 84, 1895–1901.

429
 430 **List of figure captions**
 431

- 432 Figure 1. Time evolution of the site occupancies of the Al³⁺ ion in the F39 (◇) and in the F54 (■)
 433 sample annealed at 1000°C. Symbols denote experimental points, while the curves represent data
 434 calculated according to Scheme 2.
 435
- 436 Figure 2. Time evolution of the site occupancies of the Mg²⁺ ion in the F39 (◇) and in the F54 (■)
 437 sample annealed at 1000°C. Symbols denote experimental points, while the curves represent data
 438 calculated according to Scheme 2.
- 439 Figure 3. Time evolution of the site occupancies of the Fe³⁺ ion in the F39 (◇) and in the F54 (■)
 440 sample annealed at 1000°C. Symbols denote experimental points, while the curves represent data
 441 calculated according to Scheme 2.
- 442 Figure 4. Variation of cell parameter with time for the F39 (◇) and the F54 (■) samples. Symbols
 443 denote experimental points, while the curves represent data calculated according to Scheme 2.
- 444 Figure 5. Arrhenius plots showing linear dependence of the logarithm of the rate constants, lnk_i,
 445 with inverse temperature, 1/T, for sample F39 and F54; error bars correspond to the standard
 446 deviation of the values obtained by simulating the kinetic profiles of the three cations according to
 447 Scheme 2.
 448
- 449 Figure 6. Activation energy values for Fe-Mg (A) and Mg-Al (B) as a function of Al and Fe
 450 content, respectively. The symbols ■ and □ denote the direct and inverse process, respectively.
 451
 452
 453

Tables

| | F39 | | | F54 | | |
|-------------------------------------|----------------------------|----------------------------|-----------|----------------------------|----------------------------|-----------|
| | 550°C | 650°C | 750°C | 550°C | 650°C | 750°C |
| k _i (min ⁻¹) | (7.5±0.8)·10 ⁻⁴ | (1.5±0.3)·10 ⁻² | 0.25±0.04 | (7.0±0.9)·10 ⁻⁴ | (2.7±0.8)·10 ⁻² | 0.57±0.09 |
| k _i (min ⁻¹) | (3.6±0.5)·10 ⁻⁴ | (1.0±0.2)·10 ⁻² | 0.15±0.04 | (1.8±0.6)·10 ⁻⁴ | (1.6±0.6)·10 ⁻² | 0.47±0.05 |

| | | | | | | |
|---------------------------|-------------------------------|-------------------------------|-------------------|-------------------------------|-------------------------------|-----------------|
| $k_2(\text{min}^{-1})$ | $(9.0 \pm 0.8) \cdot 10^{-5}$ | $(5.0 \pm 1.0) \cdot 10^{-3}$ | 0.14 ± 0.02 | $(2.2 \pm 0.6) \cdot 10^{-4}$ | $(1.7 \pm 0.2) \cdot 10^{-2}$ | 0.42 ± 0.02 |
| $k_{-2}(\text{min}^{-1})$ | $(9.4 \pm 0.2) \cdot 10^{-6}$ | $(3.6 \pm 0.5) \cdot 10^{-4}$ | 0.011 ± 0.003 | $(2.0 \pm 0.4) \cdot 10^{-4}$ | $(1.4 \pm 0.5) \cdot 10^{-2}$ | 0.32 ± 0.02 |

454

455 Table 1. Average values of the rate constants obtained by fitting the time-course profiles reported
 456 in figures 1-3.

457

| | $E_{a1}/\text{Kj mol}^{-1}$ $Fe_M^{3+} + Mg_T^{2+} \xrightarrow{-k_1} Fe_T^{3+} + Mg_M^{2+}$ | $E_{a1}/\text{Kj mol}^{-1}$ $Fe_T^{3+} + Mg_M^{2+} \xrightarrow{-k_{-1}} Fe_M^{3+} + Mg_T^{2+}$ | $E_{a2}/\text{Kj mol}^{-1}$ $Al_M^{3+} + Mg_T^{2+} \xrightarrow{-k_2} Al_T^{3+} + Mg_M^{2+}$ | $E_{a2}/\text{Kj mol}^{-1}$ $Al_T^{3+} + Mg_M^{2+} \xrightarrow{-k_{-2}} Al_M^{3+} + Mg_T^{2+}$ | References |
|--------------------------------------|-------------------------------------------------------------------------------------------------|----------------------------------------------------------------------------------------------------|-------------------------------------------------------------------------------------------------|----------------------------------------------------------------------------------------------------|----------------------------------|
| F39 | 204 ± 9 | 212 ± 2 | 257 ± 3 | 260 ± 10 | This study |
| | | | 274 | | Princivalle et al., (2012) |
| F54 | 234 ± 2 | 274 ± 5 | 264 ± 7 | 258 ± 6 | This study |
| | | | 265 | | Princivalle et al., 2012 |
| MgFe₂O₄ | 217 | 265 | | | Harrison and Putnis (1999) |
| MgAl₂O₄ | | | 197 ± 22 | | Andreozzi and Princivalle (2002) |
| | | | 230 | | Redfern et al., (1999) |

458

459 Table 2. Activation energy values for Fe-Mg (E_{a1} and $E_{a,-1}$) and Mg-Al (E_{a2} and $E_{a,-2}$) ionic
 460 exchange reactions obtained in the present study for the F39 and F54 samples compared with the
 461 values previously obtained for the same samples and for the end-members MgFe₂O₄ and MgAl₂O₄.
 462 For the sake of clarity the processes relative to each activation energy are also reported in the table.
 463